Arthritis & Rheumatology
Vol. 71, No. 11, November 2019, pp 1801–1811
DOI 10.1002/art.41005

American College of Rheumatology
Empowering Rheumatology Professionals

Osteoclast-Derived Autotaxin, a Distinguishing Factor for Inflammatory Bone Loss

Sacha Flammier,[1] Olivier Peyruchaud,[1] Fanny Bourguillault,[1] François Duboeuf,[1] Jean-Luc Davignon,[2] Derek D. Norman,[3] Sylvie Isaac,[4] Hubert Marotte,[5] Gabor Tigyi,[3] Irma Machuca-Gayet,[1] and Fabienne Coury[6]

Objective. The severity of rheumatoid arthritis (RA) correlates directly with bone erosions arising from osteoclast (OC) hyperactivity. Despite the fact that inflammation may be controlled in patients with RA, those in a state of sustained clinical remission or low disease activity may continue to accrue erosions, which supports the need for treatments that would be suitable for long-lasting inhibition of OC activity without altering the physiologic function of OCs in bone remodeling. Autotaxin (ATX) contributes to inflammation, but its role in bone erosion is unknown.

Methods. ATX was targeted by inhibitory treatment with pharmacologic drugs and also by conditional inactivation of the ATX gene *Ennp2* in murine OCs (ΔATX^{Ctsk}). Arthritic and erosive diseases were studied in human tumor necrosis factor–transgenic ($hTNF^{+/-}$) mice and mice with K/BxN serum transfer–induced arthritis. Systemic bone loss was also analyzed in mice with lipopolysaccharide (LPS)–induced inflammation and estrogen deprivation. Joint inflammation and bone erosion were assessed by histology and micro–computed tomography. The role of ATX in RA was also examined in OC differentiation and activity assays.

Results. OCs present at sites of inflammation overexpressed ATX. Pharmacologic inhibition of ATX in $hTNF^{+/-}$ mice, as compared to vehicle-treated controls, significantly mitigated focal bone erosion (36% decrease; $P < 0.05$) and systemic bone loss (43% decrease; $P < 0.05$), without affecting synovial inflammation. OC-derived ATX was revealed to be instrumental in OC bone resorptive activity and was up-regulated by the inflammation elicited in the presence of TNF or LPS. Specific loss of ATX in OCs from mice subjected to ovariectomy significantly protected against the systemic bone loss and erosion that had been induced with LPS and K/BxN serum treatments (30% reversal of systemic bone loss [$P < 0.01$]; 55% reversal of erosion [$P < 0.001$]), without conferring bone-protective properties.

Conclusion. Our results identify ATX as a novel OC factor that specifically controls inflammation-induced bone erosions and systemic bone loss. Therefore, ATX inhibition offers a novel therapeutic approach for potentially preventing bone erosion in patients with RA.

INTRODUCTION

Rheumatoid arthritis (RA) is a chronic relapsing disease characterized by synovial inflammation, focal bone degradation, and systemic osteoporosis. Irreversible periarticular bone erosion is a hallmark of RA, which can occur soon after disease onset and correlates with the severity of the disease and functional deterioration. At the present time, treatments

Supported by the Agence Nationale de la Recherche (project ANR-15-CE14-0010-01), Fondation ARC pour la Recherche sur le Cancer (grant PJA-20151203151), INSERM, Ligue Contre le Cancer, and Pfizer.

[1]Sacha Flammier, PhD, Olivier Peyruchaud, PhD, Fanny Bourguillault, MS, François Duboeuf, PhD, Irma Machuca-Gayet, PhD: INSERM UMR 1033 LYOS and University of Lyon I, Lyon, France; [2]Jean-Luc Davignon, MD, PhD: University of Paul Sabatier Toulouse III, INSERM-CNRS U1043, CPTP, CHU Purpan, and Pierre Paul Riquet Hospital, Toulouse, France; [3]Derek D. Norman, PhD, Gabor Tigyi, PhD: University of Tennessee Health Sciences Center, Memphis; [4]Sylvie Isaac, MD: Lyon Sud Hospital, Pierre-Bénite, France; [5]Hubert Marotte, MD, PhD: SAINBIOSE, INSERM, U1059, LBTO, University of Lyon, and University Hospital of St. Étienne, St. Étienne, France; [6]Fabienne Coury, MD, PhD: INSERM UMR 1033 LYOS and University of Lyon I, Lyon, France, and Lyon Sud Hospital, Pierre-Bénite, France.

Drs. Flammier, Peyruchaud, Machuca-Gayet, and Coury contributed equally to this work.

Dr. Marotte has received consulting fees from AbbVie, Biogen, Biogaran, Bristol-Myers Squibb, Janssen, Eli Lilly, MSD, Novartis, Pfizer, and Sanofi (less than $10,000 each) and has received research support from AbbVie, MSD, Nordic Pharma, Pfizer, Sanofi, and UCB. Dr. Coury has received consulting fees from AbbVie, Bristol-Myers Squibb, Janssen, Eli Lilly, MSD, and Pfizer (less than $10,000 each) and has received research support from AbbVie, Biogen, and Pfizer. No other disclosures relevant to this article were reported.

Address correspondence to Irma Machuca-Gayet, PhD, or Fabienne Coury, MD, PhD, INSERM UMR1033, Faculté de Médecine Lyon Est, Rue Guillaume Paradin, 69372 Lyon Cedex 08, France. E-mail: irma.machuca-gayet@inserm.fr or fabienne.coury-lucas@chu-lyon.fr.

Submitted for publication October 23, 2018; accepted in revised form May 29, 2019.

for RA are focused on the inhibition of inflammation to halt synovitis and subsequent progression of bone erosion. However, some patients in sustained clinical remission still develop radiographic erosions (1,2).

Osteoclasts (OCs) are responsible for focal erosions, juxtaarticular bone loss, and systemic osteoporosis in RA (3–5). Significant evidence has accumulated to demonstrate that OCs are present at sites of focal bone erosion at the pannus–bone interface (3,6–8). These multinucleated cells originate from fusion of myeloid cells under the control of RANKL and proinflammatory cytokines in RA (5). The aim of current treatments for RA is largely limited to controlling immune inflammation, in order to halt synovitis and to delay or even stop the subsequent progression of bone erosion. Denosumab, a neutralizing antibody that selectively binds RANKL and consequently inhibits OC formation, slows the progression of bone erosion in RA patients without affecting synovial inflammation, suggesting that it is possible to limit bone erosion by targeting OCs (9,10). However, current antiresorptive drugs are suboptimal in RA, as they could lead to atypical fractures resulting from the shutdown of physiologic bone remodeling. Therefore, there is a need for alternative therapies.

Autotaxin (ATX), also known as ecto-nucleotide pyrophosphatase/phosphodiesterase 2 (ENPP2), is a secreted enzyme produced by various tissues, including the brain, liver, and adipose tissue (11). ATX is also a lysophospholipase D, responsible for cleavage of lysophosphatidylcholine (LPC) to lysophosphatidic acid (LPA) that, in turn, acts as a growth factor with pleiotropic actions such as cell proliferation, differentiation, and migration via at least 6 G protein–coupled receptors ($LPA_{1–6}$) (12,13). High levels of LPA and ATX have been detected in the synovial fluid of RA patients (14–16), and LPA_1-knockout mice were reported to be protected from collagen-induced arthritis (14), suggesting that the LPA/ATX axis potentially controls the pathogenesis of inflammatory arthritis.

ATX is up-regulated by tumor necrosis factor (TNF) in synovial fibroblasts, resulting in increased levels of ATX at the site of joint inflammation in mouse models of RA (16). Thus, the contribution of ATX to synovial inflammation has been well established. In contrast, its role in the occurrence of bone erosions is not yet resolved. With respect to its mechanism of action, ATX could act either secondary to TNF-dependent inflammation or directly on osteoclast-mediated bone resorption. Evidence has shown that LPA is a serum-borne factor that is mandatory for RANKL-induced OC formation in vitro (17). Furthermore, LPA mediates OC survival (18) and controls OC resorption activity through cytoskeleton organization (19,20). However, the origin of LPA in bone is still unknown.

In the present study, we show that OCs produce functionally active ATX in murine arthritis. Using both genetic and pharmacologic approaches, we demonstrate that blocking ATX prevents systemic bone loss and bone erosion under inflammatory conditions accompanying murine RA, without interfering with physiologic noninflammatory bone remodeling. We provide evidence that OC-derived ATX is a key regulator whose inhibition uncouples inflammation from bone resorption. Therefore, ATX is a promising therapeutic target for the prevention of inflammation-associated bone loss and bone erosion in patients with RA.

MATERIALS AND METHODS

Mice. *Enpp2*$^{fl/fl}$ mice were kindly provided by Dr. W. H. Moolenaar (NKI, Amsterdam, The Netherlands) (21). The *Enpp2*^{fl} allele was deleted specifically in OCs by crossing this strain with mice that express the Cre recombinase under the control of the cathepsin K promoter (kindly provided by Dr. S. Kato, Tokyo University, Tokyo, Japan) (22). *Tg197* humanized TNF–transgenic (*hTNF*$^{+/–}$) mice with spontaneous arthritis were obtained from Dr. G. Kollias (A. F. B. S. Center, Athens, Greece) (23). The *Enpp2*$^{fl/fl}$ and Ctsk-Cre$^{+/–}$ mouse strains were maintained on a BALB/c genetic background, while the *hTNF*$^{+–}$ mouse strain was on the C57BL/6 background.

Four-month-old female control (*CTRL*) mice (*Enpp2*$^{fl/fl}$*Ctsk-Cre*$^{–/–}$) and Δ*ATX*^{Ctsk} mice (*Enpp2*$^{fl/fl}$*Ctsk-Cre*$^{+/–}$) underwent ovariectomy or sham surgery. After 1 month, the mice were euthanized, in accordance with the Animals in Research: Reporting In Vivo Experiments guidelines, and uterine weight was measured at necropsy. All experimental protocols were approved by the local ethics committee, CECCAPP of the École Normale Supérieure, or by the Institutional Animal Care and Use Committee of the Université Claude Bernard Lyon-1 (Lyon, France).

Animal models of inflammation and arthritis. Six-week-old male *CTRL* and Δ*ATX*^{Ctsk} mice were injected intraperitoneally (IP) with either 5 mg/kg lipopolysaccharide (LPS; Sigma-Aldrich) or a phosphate buffered saline (PBS) vehicle on day 0 and day 4. The animals were euthanized on day 8.

Animal models of both inducible arthritis and spontaneous arthritis were used in this study. K/BxN serum–transfer arthritis was induced in 7-week-old male mice, in a manner as previously described (24), by IP injection of 7 μl/gram of pooled K/BxN arthritogenic serum on days 0, 2, 7, and 12; the mice were euthanized on day 17 after the initial injection. In addition, 23-day-old *hTNF*$^{+/–}$ female mice (23) were injected IP daily with either the ATX inhibitor BMP22 (1 mg/kg/day) or PBS vehicle for 14 days; the mice were euthanized on day 14 after the first injection.

Disease severity and weight loss in both arthritis models were monitored in a blinded manner every 2–3 days by a single investigator (SF). The clinical arthritis score was assessed on a scale of 0–4, using the following scoring system: 0 = normal; 1 = mild redness or swelling of the digits, midfoot, or ankle; 2 = moderate inflammation of the digits, midfoot, or ankle; 3 = moderate-to-severe inflammation involving the digits; and 4 = severe inflammation of the entire paw, resulting in ankylosis. Each hind limb was graded, giving a maximum possible clinical arthritis score of 8 per animal. A micrometer caliper was used to measure ankle thickness (25).

Quantitative micro–computed tomography (micro-CT). Micro-CT analyses of the talus or calcaneus and of the distal femur of arthritic mice were carried out using a micro-CT scanner (Skyscan 1176). The radiographic excitation voltage was set to 50 kV with a current of 500 mA. A 0.5-mm aluminum filter was used to reduce beam-hardening artifacts. Samples were scanned in 70% ethanol with a voxel size of 9.08 μm. Section images were reconstructed with NRecon software (version 1.6.1.8; Skyscan). Three-dimensional modeling and analysis of bone volume/tissue volume (BV/TV; bone volume density) and bone surface/tissue volume (BS/TV; bone surface density) were obtained with CTAn software (version 1.9) and CTVol software (version 2.0). TV was determined as the volume of tissue in the absence of erosions, and bone surface density was used to measure surface roughness/erosion as described by Quan et al (26).

Histologic analysis. Mouse joint tissue and bone samples were fixed, decalcified, and embedded in paraffin. Cytochemical detection of tartrate-resistant acid phosphatase (TRAP)–positive OCs was performed using a TRAP activity kit assay (Sigma-Aldrich), and immunohistochemical detection of ATX was done using a polyclonal anti-ATX antibody (Cayman Chemical). The ratio of TRAP-positive OC trabecular bone surface to total trabecular bone surface (Oc.S/BS) was calculated using ImageJ software (NIH). Inflammation and bone erosions were assessed on hematoxylin–phloxine–saffron–stained sagittal sections of the midfoot, carried out in a blinded manner by 2 independent reviewers (OP and FC) using a semiquantitative scoring system, as previously described (7). Scores for inflammation and bone resorption were each assessed on a scale of 0–5, representing ascending scores of severity.

Osteoclastogenesis and bone resorption assays. Murine osteoclastogenesis and bone resorption assays were carried out as described previously (20,27). Briefly, bone marrow–derived mononuclear cells (BMMCs) from the hind limbs of mice were collected and seeded in 96-well tissue culture plates at a density of 2×10^4 cells per well in α-minimum essential medium (Invitrogen). We used charcoal-stripped fetal bovine serum to avoid contaminations of the cell culture medium with LPA and LPC. The culture medium was left untreated or supplemented with LPC (1 μ*M*; Avanti Polar Lipids), recombinant ATX (rATX; 0.3 n*M*), Ki16425 (10 μ*M*; Interchim), or PF-8380 (10 n*M*; Cayman Chemical). After 6 days, mature OCs were enumerated under a microscope on the basis of the number of nuclei (≥3 nuclei) and the extent of TRAP activity (Sigma-Aldrich). Results were expressed as the number of OCs per well.

For stimulation experiments, OCs were stimulated for 6 hours with recombinant mouse TNF (R&D Systems) or LPS (Sigma-Aldrich) after 1 hour of serum starvation in the presence or absence of TCPA-1 (2 μ*M*; Sigma-Aldrich). All osteoclastogenesis experiments were performed in triplicate.

For resorption experiments, resorbed surface was quantified on a bone-mimicking Osteo Assay Surface (3988; Corning). OCs from day 4 were detached from their plastic wells by flushing, after incubation at 37°C for 5 minutes in PBS with 0.25 m*M* EDTA. The OCs were counted and seeded at the same number (2×10^4 cells/well in 96-well plates) in replicate plates, and then cultured for 48 hours. To measure the total surface of the resorbed matrix, OCs were washed off with distilled water, and then the matrix was stained with a 5% (weight/volume) silver nitrate solution. Finally, the resorption index was obtained by calculating the total resorbed area per well. Images of all substrates were numerized with an Epsilon Perfection V750 Pro scanner (Micro Epsilon), and manually quantified with ImageJ.

Western blotting. The protein concentration of the cell extracts was determined with a Bio-Rad Protein Assay kit. Cellular extracts from cultured OCs were separated by 8% sodium dodecyl sulfate–polyacrylamide gel electrophoresis, and transferred to an Immobilon transfer membrane (Millipore). Membranes were incubated with 5% low-fat milk and 0.1% Triton X-100, pH 7.4, in PBS for 1 hour at room temperature, followed by overnight incubation with an anti-ATX antibody (Cayman Chemical) or with an anti–β-actin antibody (Sigma-Aldrich). ATX and β-actin were visualized with enhanced chemiluminescence (Amersham) using horseradish peroxidase–conjugated donkey anti-rabbit IgG or anti-mouse IgG (Jackson ImmunoResearch).

Real-time quantitative polymerase chain reaction (RT-qPCR) analysis. Total RNA from OC cultures and from powdered whole bone was extracted using TRIzol (Invitrogen) and a Nucleospin RNAII kit (Macherey-Nagel). Complementary DNA (cDNA) from OCs and bones were synthesized by reverse transcription using an iScript cDNA Synthesis kit (Bio-Rad). Expression of target genes was quantified by qRT-PCR on a Bio-Rad CFX Connect Real Time system using iTaq Universal SYBR Green Super Mix (Bio-Rad) and sets of specific primers. Values for gene quantification were normalized to the corresponding RNA L32 values, and results are expressed as the relative gene expression using the $2^{-\Delta\Delta Ct}$ method (27). Primer sequences were as follows: for *L32*, forward 5′-CAAGGAGCTGGAGGTGCTGC-3′ and reverse 5′-CTGCTCTTTCTACAATGGC-3′; for *Enpp2*, forward 5′-GCCCTGATGTCCGTGTATCT-3′ and reverse 5′-CGTTTGAA GGCAGGGTACAT-3′; for *Ctsk*, forward 5′-GAGGGCCAACTCA AGAAGAA-3′ and reverse 5′- GCCGTGGCGTTATACATACA-3′; for *Acp5*, forward 5′-CAGCAGCCCAAAATGCCT-3′ and reverse 5′-TTTTGAGCCAGGACAGCTGA-3′.

Statistical analysis. Differences between groups were determined by one-way or two-way analyses of variance followed by Bonferroni's post hoc test, using GraphPad Prism version 5.0c

software. Single comparisons were carried out using 2-sided, unpaired Mann-Whitney tests. *P* values less than or equal to 0.05 were considered significant.

RESULTS

Reduced TNF-induced focal erosion and systemic bone loss, but no interference with synovitis, following pharmacologic inhibition of ATX activity. TNF plays an important role in the initiation and progression of inflammation and destructive bone loss in RA. To evaluate the therapeutic utility of inhibiting ATX in inflammatory arthritis, we blocked ATX activity using a small molecule inhibitor, BMP22, in a model of inflammatory arthritis driven by TNF overexpression, the *hTNF*$^{+/-}$ mouse (23). The therapeutic potential of blocking ATX activity with BMP22 has been previously demonstrated in non-inflammatory mouse models (28,29). We observed that, compared to vehicle-treated controls, treatment of *hTNF*$^{+/-}$ mice with 1 mg/kg/day BMP22 for 14 days did not substantially affect inflammation, as monitored by the amount of weight loss, extent of paw swelling, clinical arthritis scores, and histopathologic features in the hind paws (Figures 1A and B). Nevertheless, the histopathologic bone erosion score was significantly reduced in BMP22-treated mice (Figure 1B).

In support of these observations, micro-CT analysis and BS/TV quantification in the calcaneum of *hTNF*$^{+/-}$ mice revealed that BMP22 was significantly protective against cortical bone erosion (36% decrease in BS/TV compared to vehicle-treated controls; $P < 0.05$) (Figure 1C). Furthermore, BMP22 treatment significantly decreased TNF-induced systemic bone loss, as indicated by a significant increase of 43% in the trabecular BV/TV in BMP22-treated mice compared to vehicle-treated mice ($P < 0.05$) (Figure 1D). Consistently, the number of TRAP-positive multinucleated OCs was significantly reduced in the long bones of *hTNF*$^{+/-}$ mice treated with BMP22 compared to vehicle-treated mice (Figure 1E).

To determine the origin of ATX in the osteoarticular environment, we analyzed serial histologic sections from *hTNF*$^{+/-}$ mice and found that expression of ATX was high at the site of synovial

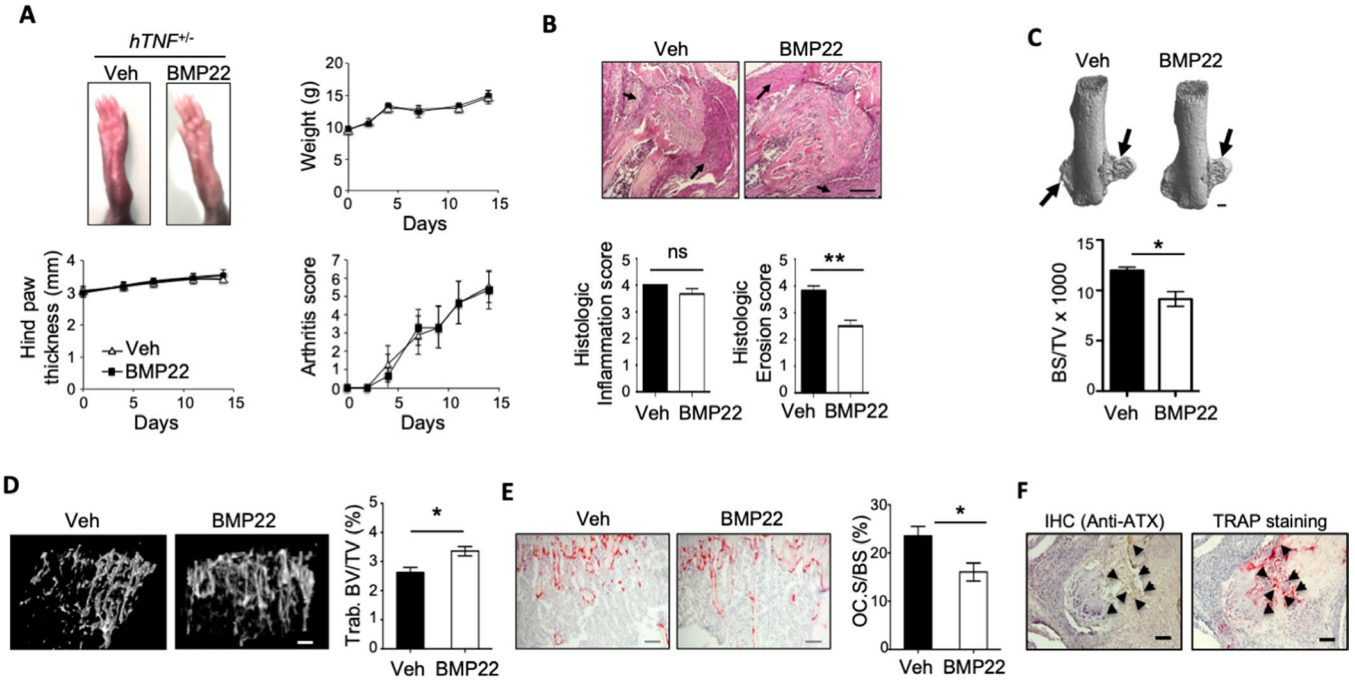

Figure 1. Blockade of autotaxin (ATX) activity has no protective effect on tumor necrosis factor (TNF)–induced synovitis but reduces TNF-induced bone erosion and systemic bone loss. **A**, Top left, Representative images of hind paw swelling in human TNF–transgenic (*hTNF*$^{+/-}$) mice 14 days after initiation of vehicle (Veh) or BMP22 treatment. Top right and bottom, Weight, hind paw thickness, and clinical arthritis scores in *hTNF*$^{+/-}$ mice during the treatment period. **B**, Top, Representative hematoxylin–phloxine–saffron staining of hind paws from a vehicle-treated and a BMP22-treated *hTNF*$^{+/-}$ mouse. **Arrows** indicate synovitis. Bottom, Histologic scores of inflammation (left) and bone erosion (right) in the midfoot of the hind paws of *hTNF*$^{+/-}$ mice. Values in **A** and **B** are the mean ± SEM of 9 mice per group. **C**, Top, Representative 3-dimensional micro–computed tomography (micro-CT) reconstruction images of the calcaneus. **Arrows** indicate areas of erosion. Bottom, Bone surface/tissue volume (BS/TV) of the calcaneus. **D**, Left, Representative 3-dimensional micro-CT reconstructions of the femoral trabecular (Trab.) bone. Right, Bone volume/tissue volume (BV/TV) of the distal femoral metaphysis. **E**, Left, Representative tartrate-resistant acid phosphatase (TRAP) staining of the tibiae. Right, Quantification of TRAP-positive surface osteoclasts (OCs) per bone surface (Oc.S/BS). Values in **C**–**E** are the mean ± SEM of 6 *hTNF*$^{+/-}$ mice per group. **F**, Representative images of immunochemical (IHC) detection of ATX (left) and TRAP staining (right) of OCs from the hind paws of *hTNF*$^{+/-}$ mice. **Arrowheads** indicate ATX-positive or TRAP-positive multinucleated cells. Bars = 100 μm. * = $P < 0.05$; ** = $P < 0.01$, by Mann-Whitney test. NS = not significant.

inflammation (Figure 1F, left). Strikingly, at the bone erosion sites in the vicinity of synovial inflammation, TRAP-positive multinucleated OCs displayed strong ATX expression (Figure 1F, right).

Functionally active role of OC-derived ATX in resorbing OCs. ATX was found to be a late marker of OC differentiation, as shown by the increased expression of the *Enpp2* gene and ATX protein during osteoclastogenesis, reaching the highest level on day 5 in mature OCs in vitro (Figure 2A).

ATX generates LPA, leading to activation of LPA receptors (30). We have previously demonstrated that LPA is a serum-borne factor required in vitro for RANKL-mediated osteoclastogenesis and osteoclastic bone resorption via activation of the LPA_1 receptor (17,20). Therefore, we investigated whether ATX expressed by OCs could affect OC differentiation and bone resorption. LPA and LPA precursors, such as LPC, are abundant in the serum; therefore, all OC manipulations were performed in the presence of charcoal-treated serum in order to eliminate the lipid fraction. Under these conditions, osteoclastogenesis and mineral matrix resorption were abrogated (Figures 2B and C). In this system, using wild-type BMMCs, no increase in the number of OCs was observed when LPC, the substrate of ATX, was added to the culture medium, indicating that OC-derived ATX failed to affect osteoclastogenesis directly (Figure 2B). This can potentially be explained by the low levels of ATX expression at early stages of OC differentiation (Figure 2A).

Nevertheless, the combination of LPC and exogenous rATX restored almost 80% of the osteoclastogenesis observed with non-delipidated serum. The effect of LPC plus rATX was completely abolished in the presence of either the ATX inhibitor PF-8380 or the $LPA_{1/3}$ antagonist Ki16425 (Figure 2B). These results indicate that ATX present in the OC environment generates functionally active LPA, which in turn regulates osteoclastogenesis.

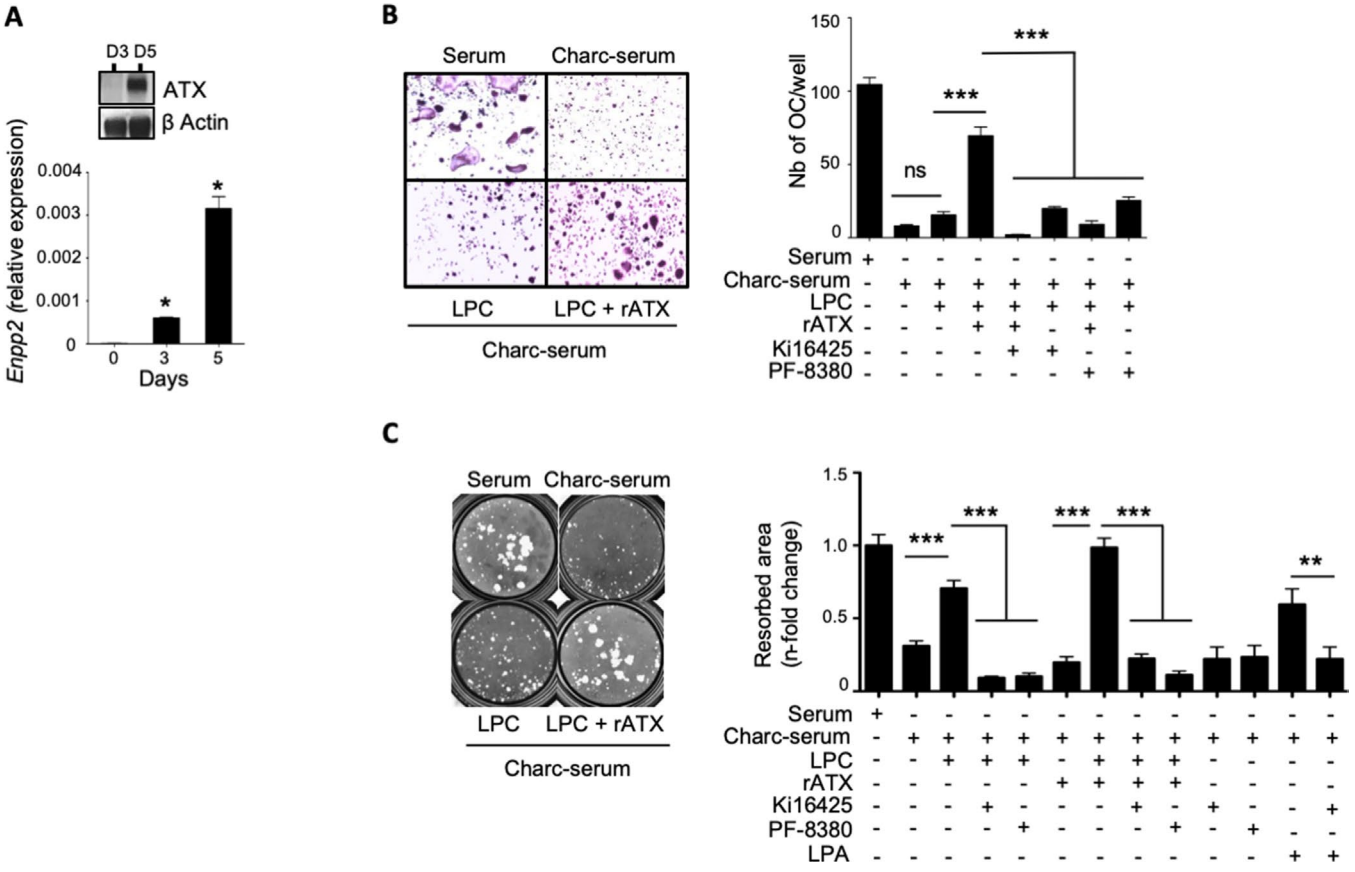

Figure 2. Autotaxin (ATX) is expressed by mature osteoclasts (OCs) and is functionally active in resorbing OCs. **A**, Top, Immunoblot analysis of cell lysates on days 3 and 5 from mature murine OCs using an ATX antibody (with β-actin as a loading control). Bottom, Quantitative reverse transcription–polymerase chain reaction analysis for the expression of *Enpp2* at different time points of differentiation of murine bone marrow–derived mononuclear cells (BMMCs) into OCs upon stimulation with macrophage colony-stimulating factor (M-CSF) and RANKL. Values are the mean ± SEM of 3 independent experiments. * = $P < 0.05$ versus day 0. **B**, Tartrate-resistant acid phosphatase (TRAP) staining (original magnification x 10) (left) and quantification (right) of OCs generated from murine BMMCs, which were cultured with M-CSF and RANKL in untreated serum or charcoal-stripped serum (Charc-serum) supplemented with the indicated compounds (lysophosphatidylcholine [LPC] alone or with recombinant ATX [rATX]) and indicated inhibitors (ATX inhibitor PF-8380 or lysophosphatidic acid [LPA] 1/3 antagonist Ki16425). **C**, Microscopic images of the resorbed mineralized well surface by murine OCs (left), and quantification based on an 8-well average per condition (right). Values in **B** and **C** are the mean ± SEM representative results from 3 independent experiments. ** = $P < 0.01$; *** = $P < 0.001$, by analysis of variance. NS = not significant.

With regard to bone resorptive activity, mature OCs were generated first in the presence of normal serum, and then re-plated on synthetic mineralized surfaces in the presence of charcoal-stripped serum. Under these conditions, LPC alone was remarkably potent in restoring 80% of the lost resorptive activity of wild-type OCs generated in charcoal-treated serum (Figure 2C). An additional enhancement of 20% in restoring bone resorptive activity was observed in OCs in the presence of LPC supplemented with rATX, suggesting that endogenous ATX produced by OCs was the most effective. PF-8380 and Ki16425 treatments abolished the effects of exogenous LPC or LPC plus rATX, and rATX by itself had no effect (Figure 2C). These data indicate that OC-derived ATX is not required during the initial steps of osteoclastogenesis, but subsequently generates functionally active LPA that promotes bone resorption by mature OCs by acting via the LPA_1 receptor.

Lack of effect of selective inhibition of OC-derived ATX on physiologic bone mass and ovariectomy-induced bone loss. To further elucidate the role of ATX in OCs, we generated mice lacking ATX in mature OCs by crossing *Enpp2*$^{fl/fl}$ mice with *Ctsk-Cre*$^{+/-}$ mice. These conditional-knockout *Enpp2*$^{fl/fl}$ *Ctsk-Cre*$^{+/-}$ mice (referred to as Δ*ATX*^{Ctsk} mice) were born at the expected birth rate (data not shown), in contrast that seen in germline-deficient *Enpp2* mice, which display a high rate of mortality during embryogenesis due to severe vascular

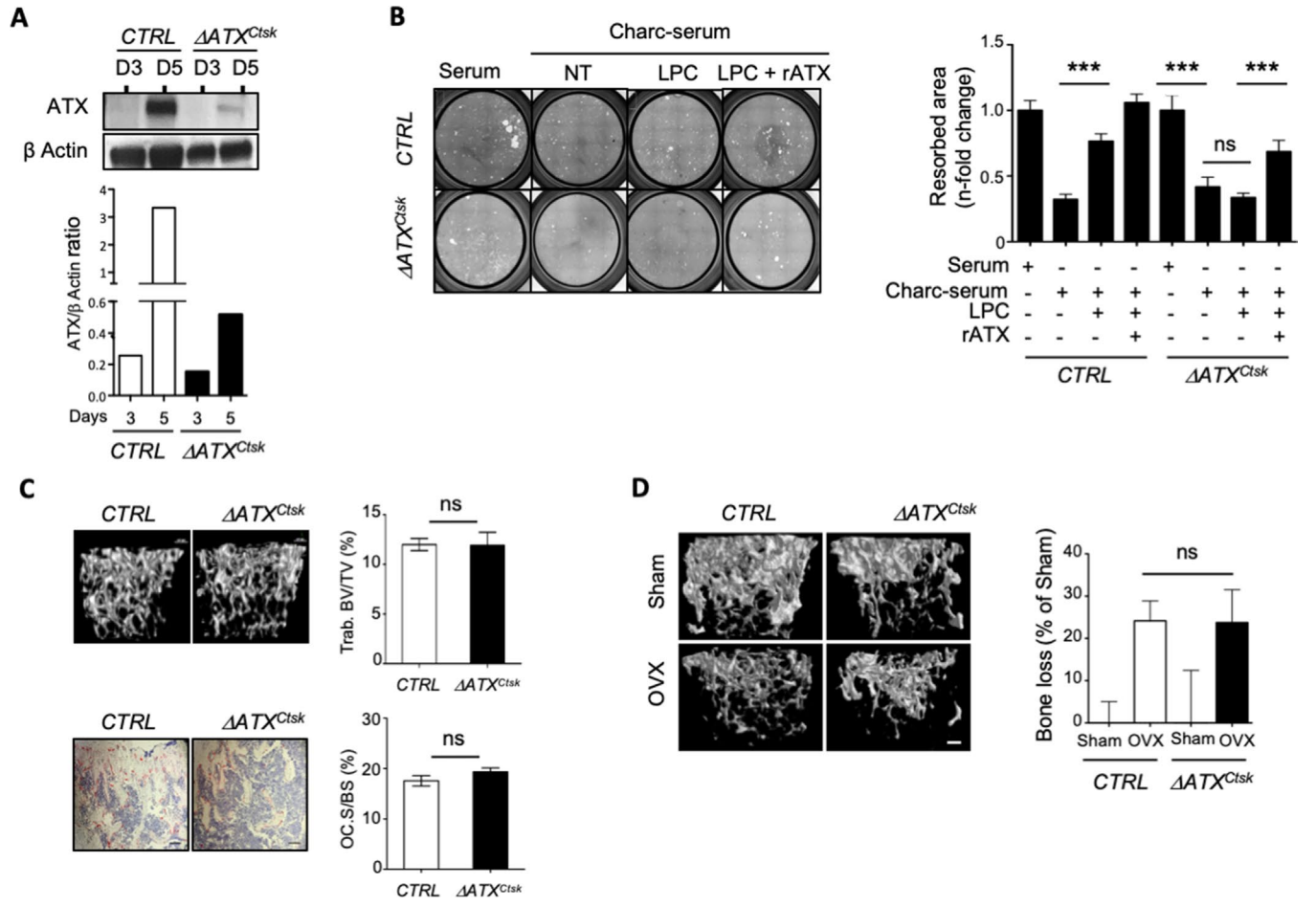

Figure 3. Inhibition of OC-derived ATX expression does not affect bone mass under basal conditions or conditions of noninflammatory osteoporosis. **A**, Cell lysates analyzed by immunoblotting with an ATX antibody (with β-actin as a loading control) (top) and quantification of the ATX to β-actin ratio (bottom) at different time points of differentiation of murine BMMCs into OCs from control mice and mice with conditional knockout of the ATX gene. **B**, Microsopic images (left) and quantification (right) of the resorbed mineralized surface by OCs generated from BMMCs of *CTRL* and Δ*ATX*^{Ctsk} mice, which were cultured with M-CSF and RANKL in untreated serum or charcoal-stripped serum supplemented with LPC with or without rATX or left not treated (NT). **C**, Top, Representative 3-dimensional micro–computed tomography (micro-CT) reconstruction images (left) and quantification of trabecular (Trab.) bone mass (bone volume/total volume [BV/TV]) (right) of *CTRL* and Δ*ATX*^{Ctsk} mice. Bottom, Representative TRAP staining (left) and quantification of TRAP-positive surface OCs per bone surface (Oc.S/BS) (right) in the tibiae of *CTRL* and Δ*ATX*^{Ctsk} mice. Values in **A–C** are the mean ± SEM of 5 mice per group. **D**, Representative 3-dimensional micro-CT reconstruction images of the trabecular bone of *CTRL* and Δ*ATX*^{Ctsk} mice after ovariectomy (OVX) or sham operation (left) and quantification of trabecular bone loss as a percentage of the BV/TV of sham-operated animals (right). Values are the mean ± SEM of 9 mice per group. *** = $P < 0.001$ by analysis of variance. Bars = 100 μm. See Figure 2 for other definitions.

and neuronal defects (21,31). ATX expression was assessed in vitro during the differentiation of BMMCs into OCs. We found an almost complete absence of the protein in the mature OCs (Figure 3A). Consistent with the previous results on bone resorption in wild-type mouse OCs in the presence of the ATX inhibitor (Figure 2C), ATX-deficient mouse OCs were unable to resorb mineralized matrix in the presence of LPC alone, whereas the addition of rATX rescued this phenotype (Figure 3B).

Surprisingly, quantitative micro-CT measurements of the bone density and quantification of the OC numbers in *CTRL* mice and Δ*ATX*^{Ctsk} mice did not reveal any differences (Figure 3C). Remarkably, sham-operated and ovariectomized *CTRL* and Δ*ATX*^{Ctsk} mice did not show any differences in bone volume density as measured by micro-CT (Figure 3D). Thus, selective deletion of OC-derived ATX appears to have no impact on bone mass under either nonpathologic physiologic conditions or pathologic conditions of ovariectomy-induced osteoporosis.

Prevention of LPS-induced bone loss with selective inhibition of OC-derived ATX. Because pharmacologic inhibition of ATX activity protected *hTNF*$^{+/-}$ mice from bone erosion and systemic bone loss (Figure 1), we hypothesized that potential regulation of bone mass by ATX might manifest only under inflammatory conditions. We first generated and harvested mature

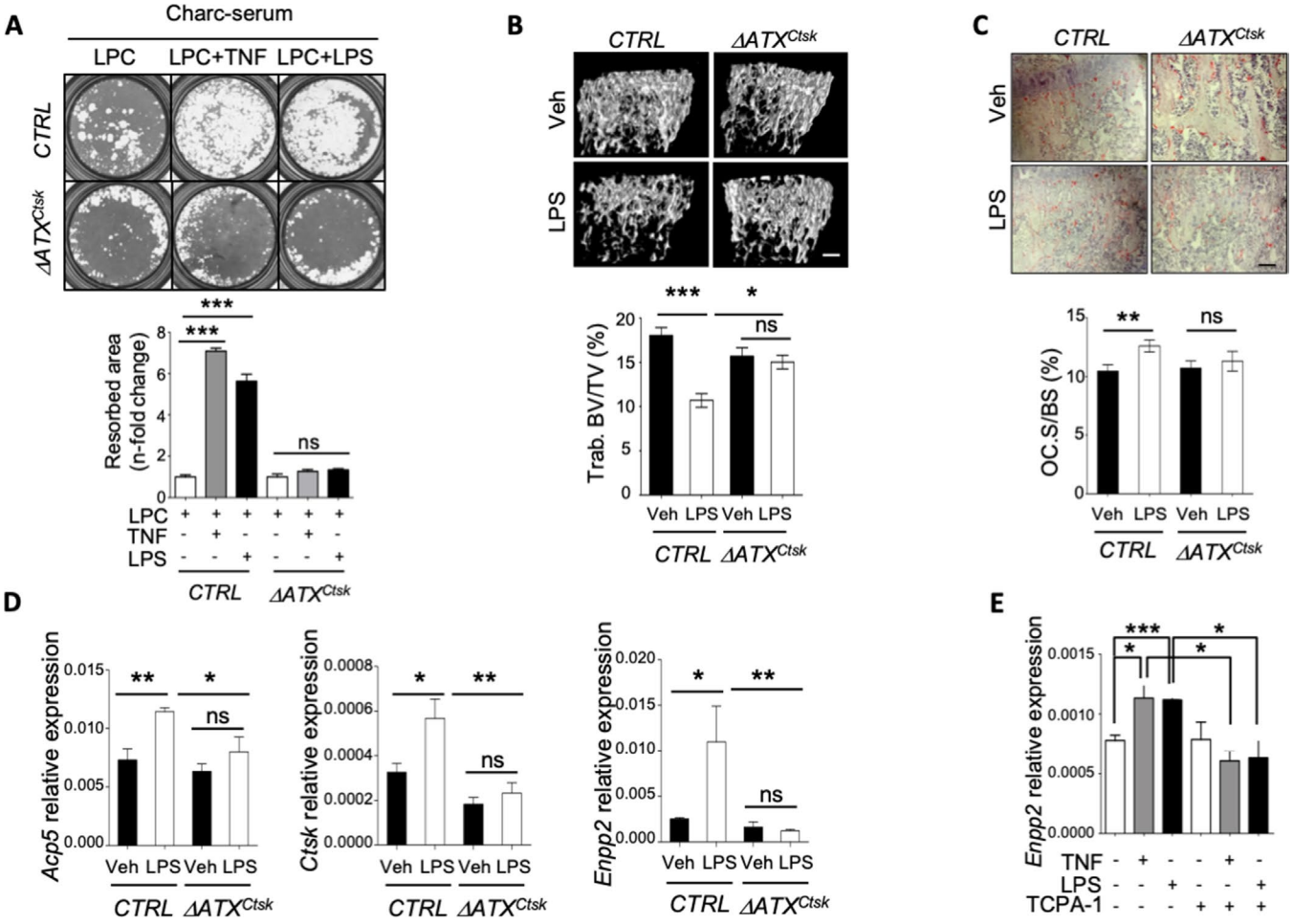

Figure 4. Inhibition of OC-derived ATX expression fully protects mice against lipopolysaccharide (LPS)–induced bone loss. **A**, Microscopic images (top) and quantification (bottom) of the resorbed mineralized surface by OCs generated from BMMCs of control mice and mice with conditional knockout of the ATX gene, which were cultured with M-CSF and RANKL and seeded for 48 hours in osteo-assay wells in charcoal-stripped serum supplemented with LPC alone or together with tumor necrosis factor (TNF) (10 ng/ml) or LPS (1 μg/ml). **B**, Representative 3-dimensional micro–computed tomography reconstruction images (top) and quantification of femoral trabecular (Trab.) bone mass (bone volume/total volume [BV/TV]) (bottom) of *CTRL* and Δ*ATX*^{Ctsk} mice treated with either LPS or vehicle (Veh). **C**, Representative TRAP staining (top) and quantification of TRAP-positive surface OCs per bone surface (Oc.S/BS) (bottom) in the tibiae of *CTRL* and Δ*ATX*^{Ctsk} mice treated with either LPS or vehicle. **D**, Quantitative reverse transcription–polymerase chain reaction (RT-PCR) analysis of the expression of *Acp5, Ctsk*, and *Enpp2* in the long bones of *CTRL* and Δ*ATX*^{Ctsk} mice treated with either LPS or vehicle. **E**, Quantitative RT-PCR analysis of the expression of *Enpp2* in mature BMMC-derived OCs from *CTRL* mice, stimulated for up to 6 hours with TNF (10 ng/ml) or LPS (1 μg/ml) with or without TCPA-1 (2 μ*M*). Values are the mean ± SEM of 6 mice per group. Bars = 100 μm. * = $P < 0.05$; ** = $P < 0.01$; *** = $P < 0.001$, by analysis of variance. See Figure 2 for other definitions.

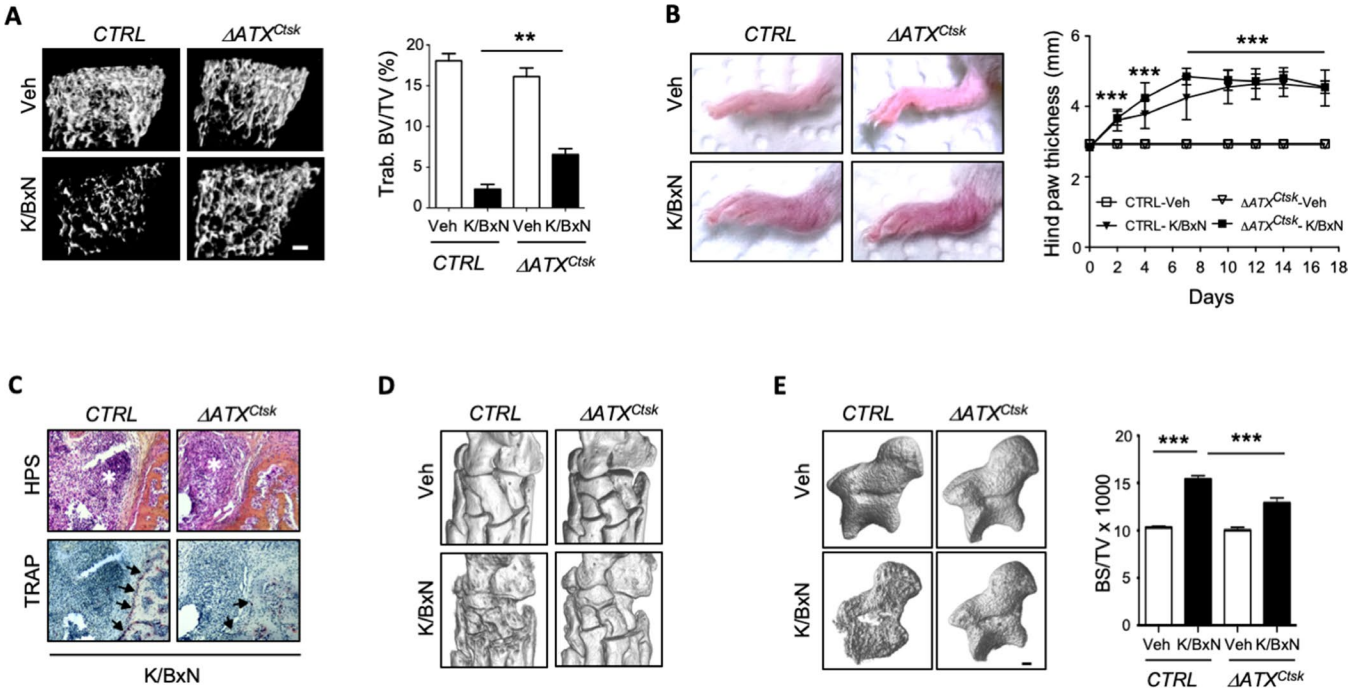

Figure 5. Mice deficient in OC-derived ATX are partially protected against K/BxN serum transfer–induced bone erosion and systemic bone loss. **A**, Representative 3-dimensional micro–computed tomography (micro-CT) reconstruction images (left) and quantification (right) of femoral trabecular (Trab.) bone mass (bone volume/total volume [BV/TV]) of control mice and mice with conditional knockout of the ATX gene treated with K/BxN serum or vehicle (Veh). Bar = 100 μm. **B**, Representative images of hind paw swelling 17 days after the initial serum transfer (left) and hind paw thickness during the K/BxN serum transfer period (right) in *CTRL* and Δ*ATX*^{Ctsk} mice treated with K/BxN serum or vehicle. **C**, Representative hematoxylin–phloxine–saffron (HPS) staining (top) and TRAP staining (bottom) of the hind paws from *CTRL* and Δ*ATX*^{Ctsk} mice treated with K/BxN serum. **Asterisks** and **arrows** indicate synovitis and TRAP-positive multinucleated cells, respectively, at the synovitis–bone interface. Bar = 100 μm. **D**, Representative 3-dimensional micro-CT reconstruction images of the hind paws 17 days after the initial serum transfer, in groups of *CTRL* and Δ*ATX*^{Ctsk} mice treated with K/BxN serum or vehicle. Original magnification = 250 μm. **E**, Representative 3-dimensional micro-CT reconstruction images (left) and bone surface/tissue volume (BS/TV) (right) of the talus from *CTRL* and Δ*ATX*^{Ctsk} mice treated with K/BxN serum or vehicle. Bar = 100 μm. Values are the mean ± SEM of 6 mice per group. ** = $P < 0.01$; *** = $P < 0.001$, by analysis of variance. See Figure 2 for other definitions.

OCs from *CTRL* and Δ*ATX*^{Ctsk} mice, which were then secondary plated on mineralized matrix in the presence of LPC and charcoal-stripped serum supplemented with or without TNF or LPS. Compared to *CTRL* mouse OCs, whose bone resorptive activity was significantly enhanced by TNF and LPS, ATX-deficient mouse OCs were refractory to stimulation by either TNF or LPS (Figure 4A).

To extend this finding in the context of inflammation-dependent OC resorption in vivo, we treated *CTRL* and Δ*ATX*^{Ctsk} mice with an endotoxin LPS challenge (5 mg/kg). As expected, in *CTRL* mice, LPS induced a drastic bone loss, with 40% reduction in the BV/TV compared to vehicle-treated mice (32). In contrast, LPS-treated Δ*ATX*^{Ctsk} mice displayed no significant trabecular bone mass reduction, with BV/TV values similar to those observed in vehicle-treated animals (Figure 4B). LPS-treated *CTRL* mice exhibited a significant increase in the Oc.S/BS compared to mice treated with vehicle, whereas Δ*ATX*^{Ctsk} mice challenged with LPS showed no change in OC content when compared to vehicle-treated Δ*ATX*^{Ctsk} mice (Figure 4C).

Furthermore, LPS treatment induced a significant increase in the expression of the late osteoclastic markers *Acp5* and *CtsK* and a significant increase in the levels of *Enpp2* in the bone from *CTRL* mice, but not in the bone from Δ*ATX*^{Ctsk} mice (Figure 4D). Remarkably, we observed a significant increase in *Enpp2* transcript levels induced by LPS in *CTRL* mice only (Figure 4D), indicating that among the bone cells expressing *Enpp2*, the OC is most responsive to LPS challenge.

To evaluate whether the inflammatory environment affected *Enpp2* expression in OCs, mature OCs from *CTRL* mice were treated with either TNF or LPS in the presence of LPC and charcoal-stripped serum. Both treatments up-regulated *Enpp2* in mature OCs, indicating that the *Enpp2* promoter was the target of TNF and LPS signaling pathways in these fully differentiated cells (Figure 4E). This hypothesis was confirmed in experiments using TCPA-1, a selective inhibitor of IκB kinase β, which completely abolished both the TNF-induced and LPS-induced expression of *Enpp2* (Figure 4E).

Impact of selective deletion of OC-derived ATX on bone mass and erosion in arthritic inflammation. We next investigated whether OC-derived ATX could contribute to

arthritis-induced bone loss. *CTRL* and Δ*ATX*^{Ctsk} mice were injected with serum from K/BxN mice to induce an arthritic disease (24). Consistent with the results obtained in the LPS model, under these extreme inflammatory conditions, micro-CT analysis showed that K/BxN serum transfer elicited a severe decrease in trabecular bone mass (88% decrease in the BV/TV) in *CTRL* mice. In contrast, serum transfer was significantly less detrimental in Δ*ATX*^{Ctsk} mice, causing a 58% decrease in the BV/TV, thereby indicating that in Δ*ATX*^{Ctsk} mice with K/BxN serum–transfer arthritis, a significant protection against systemic bone loss was conferred (30% difference in change in BV/TV versus *CTRL* mice; $P < 0.01$) (Figure 5A).

Of note, the extent of paw swelling, clinical arthritis scores, and histologic severity of synovitis were comparable between Δ*ATX*^{Ctsk} mice and *CTRL* mice treated with K/BxN serum, underscoring that OC-derived ATX does not impact the inflammatory process (Figures 5B and C). Remarkably, Δ*ATX*^{Ctsk} mice displayed less TRAP-positive multinucleated OCs at the synovitis–bone interface than did *CTRL* mice, and Δ*ATX*^{Ctsk} mice displayed significative protection against the cortical erosion induced by K/BxN serum (Figures 5C and D).

Talus BS/TV values in *CTRL* mice treated with K/BxN serum showed a significant increase of 1.8-fold as compared to that in vehicle-treated controls. Elevation of the BS/TV ratio was attributed to an increase in bone surface, which was dependent on roughness and bone cortical erosions. Remarkably, the increase in talus BS/TV values in Δ*ATX*^{Ctsk} mice induced by K/BxN serum transfer was significantly reduced, by 55%, compared to that in *CTRL* mice ($P < 0.001$) (Figure 5E).

Taken together, these results indicate that OC-derived ATX did not contribute to the inflammatory process but did control arthritic bone destruction. These findings highlight the possibility that ATX could serve as a novel therapeutic target for the control of RA-associated bone loss.

DISCUSSION

The hypothesis addressed herein, suggesting a major contribution of LPA and ATX in RA, has emerged recently (14,16). Mice with global deletion of the *Lpar1* gene do not develop arthritis following immunization with type II collagen, because immune cell infiltration is mitigated (14). By using these LPA_1-deficient mice and pharmacologic LPA_1-blocking drugs, we have previously shown that this receptor is a key effector of OC-mediated bone resorption (20). In addition, TNF-driven ATX expression in synovial fibroblasts generates LPA that, in turn, activates synovial fibroblasts (14,16). Thus, combined LPA and TNF signaling might contribute to joint inflammation and, potentially, to joint destruction. Indeed, genetic and pharmacologic targeting of LPA_1 results in attenuated bone degradation in animal models of arthritis (14).

Data from preclinical animal arthritis models challenged with ATX inhibitor compounds have been lacking so far. Our study represents an important advance over the previously described model of conditional genetic ablation of ATX in mesenchymal cells (16). The hypothesis put forward in that report predicted a potential attenuation of inflammation after ATX inhibitor treatment. However, in the present study, we found that treatment with the inhibitor BMP22 did not significantly affect articular inflammation in *hTNF*$^{+/-}$ mice. This finding could have been attributable to a suboptimal dosing regimen. However, BMP22-treated *hTNF*$^{+/-}$ mice displayed a significant reduction in local bone erosion and systemic bone loss. Thus, pharmacologic inhibition of ATX with BMP22 protected *hTNF*$^{+-}$ mice from inflammation-induced bone loss by mitigating osteoclastic bone resorption, rather than by affecting the inflammatory response. Therefore, inhibition of ATX using BMP22 caused distinctively different effects on inflammation when compared to its effects on bone resorption in this model of RA.

Bone erosions constitute a key and irreversible outcome in RA and are reflective of the tight interaction between the immune system and bone remodeling. Controlling synovial inflammation can arrest the progression of bone erosions in RA. However, RA patients in sustained clinical remission or with low disease activity often continue to accrue bone erosions. In addition, certain RA patients exhibit persistent chronic synovitis that is marked by joint swelling without palpable joint tenderness (33). Therefore, it might be worthwhile to consider the development of alternative therapeutic agents that would selectively and directly target bone erosion. Indeed, current antiresorptive drugs, such as bisphosphonates and denosumab, can lead to atypical bone fractures, because long-term treatment with these drugs can shut down physiologic bone remodeling.

No induction of toxicity was observed with BMP22 in the present study, nor has there been any reports of toxicity in experimental mouse models of cancer using blockers of ATX activity (28,34,35). Furthermore, phase II clinical evaluation of GLPG1690, a first-in-class ATX inhibitor, for the treatment of idiopathic pulmonary fibrosis has been successfully completed without noted side effects (36). Therefore, pharmacologic blocking of ATX activity is likely to also be safe in RA patients.

ATX was found to be a late osteoclastic marker, explaining the absence of its impact on the differentiation of Δ*ATX*^{Ctsk} mouse OCs. In contrast, mature OCs from Δ*ATX*^{Ctsk} mice were remarkably defective in mineral matrix degradation, and this was potently rescued when exogenous ATX was added to the cell cultures. Additional sources of ATX and/or LPA might also be available in the bone microenvironment, originating from chondrocytes (37), osteoblasts (38), adipocytes (39), and endothelial cells (40), that may partly explain the absence of the bone phenotype in Δ*ATX*^{Ctsk} mice. Surprisingly, specific inhibition of OC-derived ATX did not protect Δ*ATX*^{Ctsk} mice from osteoporosis induced by ovariectomy, in striking contrast to the full protection conferred by inhibition of ATX in animals with LPS- or K/BxN serum transfer–induced bone loss. This suggests that OC-derived ATX might be central to a remarkable specificity for

inflammation over estrogen-dependent regulation of OC activity and bone degradation. Indeed, TNF and LPS enhanced the resorption activity by 6–7 fold in *CTRL* mouse OCs but were ineffective in ΔATX^{Ctsk} mouse OCs. This contention was supported by the presence of NF-κB DNA binding sites on the *Enpp2* promoter sequence (41) and was confirmed experimentally by the use of TCPA-1, a selective inhibitor of IκB kinase β, which totally blunted LPS- and TNF-enhanced ATX expression, indicating a convergent regulation mechanism for *Enpp2* expression by both LPS and TNF in mature OCs.

Collectively, our results demonstrate that osteoclast-derived ATX is a key player in inflammatory osteoclast-mediated bone resorption. Thus, ATX should be considered as a promising novel therapeutic target for halting bone erosion in patients with RA.

ACKNOWLEDGMENT

The authors thank Dr. Antonios O. Aliprantis for helpful advice.

AUTHOR CONTRIBUTIONS

All authors were involved in drafting the article or revising it critically for important intellectual content, and all authors approved the final version to be published. Drs. Machuca-Gayet and Coury had full access to all of the data in the study and take responsibility for the integrity of the data and the accuracy of the data analysis.

Study conception and design. Peyruchaud, Machuca-Gayet, Coury.

Acquisition of data. Flammier, Bourguillault, Duboeuf, Norman, Isaac, Machuca-Gayet.

Analysis and interpretation of data. Flammier, Peyruchaud, Davignon, Marotte, Tigyi, Machuca-Gayet, Coury.

ROLE OF THE STUDY SPONSOR

Pfizer provided financial support through a Passerelle grant, and facilitated the design and implementation of the study. The authors independently collected the data, interpreted the results, and had the final decision to submit the manuscript for publication. Publication of this article was not contingent upon approval by Pfizer.

REFERENCES

1. Cohen G, Gossec L, Dougados M, Cantagrel A, Goupille P, Daures JP, et al. Radiological damage in patients with rheumatoid arthritis on sustained remission. Ann Rheum Dis 2007;66:358–63.
2. Molenaar ET, Voskuyl AE, Dinant HJ, Bezemer PD, Boers M, Dijkmans BA. Progression of radiologic damage in patients with rheumatoid arthritis in clinical remission. Arthritis Rheum 2004;50:36–42.
3. Gravallese EM, Harada Y, Wang JT, Gorn AH, Thornhill TS, Goldring SR. Identification of cell types responsible for bone resorption in rheumatoid arthritis and juvenile rheumatoid arthritis. Am J Pathol 1998;152:943–51.
4. Goldring SR, Gravallese EM. Bisphosphonates: environmental protection for the joint? [editorial]. Arthritis Rheum 2004;50:2044–7.
5. Schett G, Hayer S, Zwerina J, Redlich K, Smolen JS. Mechanisms of disease: the link between RANKL and arthritic bone disease. Nat Clin Pract Rheumatol 2005;1:47–54.
6. Bromley M, Woolley DE. Chondroclasts and osteoclasts at subchondral sites of erosion in the rheumatoid joint. Arthritis Rheum 1984;27:968–75.
7. Pettit AR, Ji H, von Stechow D, Müller R, Goldring SR, Choi Y, et al. TRANCE/RANKL knockout mice are protected from bone erosion in a serum transfer model of arthritis. Am J Pathol 2001;159:1689–99.
8. Redlich K, Hayer S, Maier A, Dunstan CR, Tohidast-Akrad M, Lang S, et al. Tumor necrosis factor α–mediated joint destruction is inhibited by targeting osteoclasts with osteoprotegerin. Arthritis Rheum 2002;46:785–92.
9. Deodhar A, Dore RK, Mandel D, Schechtman J, Shergy W, Trapp R, et al. Denosumab-mediated increase in hand bone mineral density associated with decreased progression of bone erosion in rheumatoid arthritis patients. Arthritis Care Res (Hoboken) 2010;62:569–74.
10. Cohen SB, Dore RK, Lane NE, Ory PA, Peterfy CG, Sharp JT, et al, on behalf of the Denosumab Rheumatoid Arthritis Study Group. Denosumab treatment effects on structural damage, bone mineral density, and bone turnover in rheumatoid arthritis: a twelve-month, multicenter, randomized, double-blind, placebo-controlled, phase II clinical trial. Arthritis Rheum 2008;58:1299–309.
11. Giganti A, Rodriguez M, Fould B, Moulharat N, Cogé F, Chomarat P, et al. Murine and human autotaxin α, β, and γ isoforms: gene organization, tissue distribution, and biochemical characterization. J Biol Chem 2008;283:7776–89.
12. Umezu-Goto M, Kishi Y, Taira A, Hama K, Dohmae N, Takio K, et al. Autotaxin has lysophospholipase D activity leading to tumor cell growth and motility by lysophosphatidic acid production. J Cell Biol 2002;158:227–33.
13. Moolenaar WH, Hla T. Snapshot: bioactive lysophospholipids. Cell 2012;148:378.
14. Miyabe Y, Miyabe C, Iwai Y, Takayasu A, Fukuda S, Yokoyama W, et al. Necessity of lysophosphatidic acid receptor 1 for development of arthritis. Arthritis Rheum 2013;65:2037–47.
15. Zhao C, Fernandes MJ, Prestwich GD, Turgeon M, Di Battista J, Clair T, et al. Regulation of lysophosphatidic acid receptor expression and function in human synoviocytes: implications for rheumatoid arthritis? Mol Pharmacol 2008;73:587–600.
16. Nikitopoulou I, Oikonomou N, Karouzakis E, Sevastou I, Nikolaidou-Katsaridou N, Zhao Z, et al. Autotaxin expression from synovial fibroblasts is essential for the pathogenesis of modeled arthritis. J Exp Med 2012;209:925–33.
17. David M, Wannecq E, Descotes F, Jansen S, Deux B, Ribeiro J, et al. Cancer cell expression of autotaxin controls bone metastasis formation in mouse through lysophosphatidic acid-dependent activation of osteoclasts. PloS One 2010;5:e9741.
18. Lapierre DM, Tanabe N, Pereverzev A, Spencer M, Shugg RP, Dixon SJ, et al. Lysophosphatidic acid signals through multiple receptors in osteoclasts to elevate cytosolic calcium concentration, evoke retraction, and promote cell survival. J Biol Chem 2010;285:25792–801.
19. McMichael BK, Meyer SM, Lee BS. C-Src-mediated phosphorylation of thyroid hormone receptor-interacting protein 6 (TRIP6) promotes osteoclast sealing zone formation. J Biol Chem 2010;285:26641–51.
20. David M, Machuca-Gayet I, Kikuta J, Ottewell P, Mima F, Leblanc R, et al. Lysophosphatidic acid receptor type 1 (LPA1) plays a functional role in osteoclast differentiation and bone resorption activity. J Biol Chem 2014;289:6551–64.
21. Van Meeteren LA, Ruurs P, Stortelers C, Bouwman P, van Rooijen MA, Pradère JP, et al. Autotaxin, a secreted lysophospholipase D, is essential for blood vessel formation during development. Mol Cell Biol 2006;26:5015–22.
22. Nakamura T, Imai Y, Matsumoto T, Sato S, Takeuchi K, Igarashi K, et al. Estrogen prevents bone loss via estrogen receptor α and induction of Fas ligand in osteoclasts. Cell 2007;130:811–23.

23. Keffer J, Probert L, Cazlaris H, Georgopoulos S, Kaslaris E, Kioussis D, et al. Transgenic mice expressing human tumour necrosis factor: a predictive genetic model of arthritis. EMBO J 1991;10:4025–31.
24. Monach PA, Mathis D, Benoist C. The K/BxN arthritis model. Curr Protoc Immunol 2008;81:1–12.
25. Danks L, Komatsu N, Guerrini MM, Sawa S, Armaka M, Kollias G, et al. RANKL expressed on synovial fibroblasts is primarily responsible for bone erosions during joint inflammation. Ann Rheum Dis 2016;75:1187–95.
26. Quan L, Zhang Y, Dusad A, Ren K, Purdue PE, Goldring SR, et al. The evaluation of the therapeutic efficacy and side effects of a macromolecular dexamethasone prodrug in the collagen-induced arthritis mouse model. Pharm Res 2016;33:186–93.
27. Georgess D, Mazzorana M, Terrado J, Delprat C, Chamot C, Guasch RM, et al. Comparative transcriptomics reveals RhoE as a novel regulator of actin dynamics in bone-resorbing osteoclasts. Mol Biol Cell 2014;25:380–96.
28. Leblanc R, Lee SC, David M, Bordet JC, Norman DD, Patil R, et al. Interaction of platelet-derived autotaxin with tumor integrin αVβ3 controls metastasis of breast cancer cells to bone. Blood 2014;124:3141–50.
29. Gupte R, Patil R, Liu J, Wang Y, Lee SC, Fujiwara Y, et al. Benzyl and naphthalene methylphosphonic acid inhibitors of autotaxin with anti-invasive and anti-metastatic activity. Chem Med Chem 2011;6:922–35.
30. Nakanaga K, Hama K, Aoki J. Autotaxin—an LPA producing enzyme with diverse functions. J Biochem 2010;148:13–24.
31. Fotopoulou S, Oikonomou N, Grigorieva E, Nikitopoulou I, Paparountas T, Thanassopoulou A, et al. ATX expression and LPA signalling are vital for the development of the nervous system. Dev Biol 2010;339:451–64.
32. Lee JM, Park H, Noh AL, Kang JH, Chen L, Zheng T, et al. 5-lipoxygenase mediates RANKL-induced osteoclast formation via the cysteinyl leukotriene receptor 1. J Immunol 2012;189:5284–92.
33. Brown AK, Conaghan PG, Karim Z, Quinn MA, Ikeda K, Peterfy CG, et al. An explanation for the apparent dissociation between clinical remission and continued structural deterioration in rheumatoid arthritis. Arthritis Rheum 2008;58:2958–67.
34. Benesch MG, Tang X, Maeda T, Ohhata A, Zhao YY, Kok BP, et al. Inhibition of autotaxin delays breast tumor growth and lung metastasis in mice. FASEB J 2014;28:2655–66.
35. Benesch MG, Ko YM, Tang X, Dewald J, Lopez-Campistrous A, Zhao YY, et al. Autotaxin is an inflammatory mediator and therapeutic target in thyroid cancer. Endocr Relat Cancer 2015;22:593–607.
36. Desroy N, Housseman C, Bock X, Joncour A, Bienvenu N, Cherel L, et al. Discovery of 2-[[2-ethyl-6-[4-[2-(3-hydroxyazetidin-1-yl)-2-oxoethyl]piperazin-1-yl]-8-methylimidazo[1,2-a]pyridin-3-yl]methylamino]-4-(4-fluorophenyl)thiazole-5-carbonitrile (GLPG1690), a first-in-class autotaxin inhibitor undergoing clinical evaluation for the treatment of idiopathic pulmonary fibrosis. J Med Chem 2017;60:3580–90.
37. Nishioka T, Arima N, Kano K, Hama K, Itai E, Yukiura H, et al. ATX-LPA1 axis contributes to proliferation of chondrocytes by regulating fibronectin assembly leading to proper cartilage formation. Sci Rep 2016;6:23433.
38. Panupinthu N, Rogers JT, Zhao L, Solano-Flores LP, Possmayer F, Sims SM, et al. P2X7 receptors on osteoblasts couple to production of lysophosphatidic acid: a signaling axis promoting osteogenesis. J Cell Biol 2008;181:859–71.
39. Ferry G, Tellier E, Try A, Grés S, Naime I, Simon MF, et al. Autotaxin is released from adipocytes, catalyzes lysophosphatidic acid synthesis, and activates preadipocyte proliferation: up-regulated expression with adipocyte differentiation and obesity. J Biol Chem 2003;278:18162–9.
40. Kanda H, Newton R, Klein R, Morita Y, Gunn MD, Rosen SD. Autotaxin, an ectoenzyme that produces lysophosphatidic acid, promotes the entry of lymphocytes into secondary lymphoid organs. Nat Immunol 2008;9:415–23.
41. Wu JM, Xu Y, Skill NJ, Sheng H, Zhao Z, Yu M, et al. Autotaxin expression and its connection with the TNF-α-NF-κB axis in human hepatocellular carcinoma. Mol Cancer 2010;9:71.